Optics Letters

Towards power scaling of 2.8 μm fiber lasers

Yigit Ozan Aydin,* Vincent Fortin, Réal Vallée, and Martin Bernier

Centre d'optique, photonique et laser (COPL), Université Laval, Québec City, Québec G1V 0A6, Canada
**Corresponding author: yigit-ozan.aydin.1@ulaval.ca*

Received 30 July 2018; accepted 19 August 2018; posted 22 August 2018 (Doc. ID 340990); published 14 September 2018

We report the demonstration of a 2824 nm passively cooled erbium-doped fluoride fiber laser delivering a record average output power of 41.6 W in continuous-wave operation. The splice-less cavity is based on intra-core fiber Bragg gratings written directly in the active erbium-doped fluoride fiber, which is bidirectionally pumped at 980 nm to reduce heat load. To the best of our knowledge, this result is the highest average output power achieved with a mid-infrared fiber laser. The long-term performance of different protective endcaps is also investigated at high-power operation.

OCIS codes: (140.3070) Infrared and far-infrared lasers; (140.3500) Lasers, erbium; (140.3510) Lasers, fiber; (230.1480) Bragg reflectors.

https://doi.org/10.1364/OL.43.004542

Mid-infrared fiber laser sources emitting near 3 μm have made significant progress in recent years [1–3], largely due to the advent of high-quality double-clad fluoride fibers, high-power InGaAs laser diodes, and advances in fiber Bragg grating (FBG) inscription technology. Nonetheless, continuous efforts are still needed to improve their performances and meet the requirements of potential high-end applications in material processing [4], medicine [5], and defense and security [6].

Laser emission near 3 μm can be obtained with holmium- (Ho^{3+}) [7], dysprosium- (Dy^{3+}) [8], and erbium- (Er^{3+}) [9] doped fluoride fibers. However, the sources based on Ho^{3+} and Dy^{3+} are actually power limited because of the lack of high-power pump diodes. Erbium-doped fiber lasers, on the other hand, can conveniently generate high-power 3 μm emission through the $^4I_{11/2} \rightarrow {}^4I_{13/2}$ transition by using powerful commercial InGaAs laser diodes emitting around 976 nm. In this transition, the lifetime of the upper lasing level ($^4I_{11/2}$) is shorter than that of the lower lasing level ($^4I_{13/2}$). However, depleting mechanisms such as energy transfer upconversion (ETU) at high erbium concentrations [10], Pr^{3+} co-doping [11] and cascade lasing [12] are well-known solutions to depopulate the lower state of the 3 μm transition.

To date, most of the high-power demonstrations of erbium fluoride fiber lasers reported [1,10,13–15] were based on heavily doped fluoride glasses (>5 mol. %), which relied strongly on the ETU process ($^4I_{13/2}$, $^4I_{13/2}$) → ($^4I_{9/2}$, $^4I_{15/2}$) to reduce the effective lifetime of the lower lasing level. However, these active fibers usually suffer from a high heat load at the pump end due to the strong pump absorption, combined to the large quantum defect and poor thermal properties of fluoride glasses compared with silica. This issue is even more critical when the highly reflective FBG (HR-FBG) is directly written in the core of the active fiber. In fact, the large temperature increase can potentially shift its center wavelength outside the reflection band of the output FBG (LR-FBG), which can lead to instability issues and a decrease of the efficiency. For this reason, the HR-FBG is most often written in the core of a matching undoped single-mode fluoride glass fiber in high-power demonstrations [1,13,16]. However, this approach requires an additional splice between dissimilar undoped and doped single-mode fluoride fibers, which increases the round-trip losses of the cavity and, more importantly, causes local hot spots by scattering 3 μm radiation on the strongly absorbing (≈20–200 dB/mm) surrounding polymer. Thus, eliminating intracavity splices by writing FBGs in the doped fiber is advantageous to simplify the laser cavity assembly, reduce the intracavity losses, and remove potential points of failure from the system. Based on that approach, splice-less fluoride laser cavities at 2.82 and 2.94 μm have been demonstrated by Bernier *et al.* [17] and Faucher *et al.* [18], but were limited to average output powers around 5 W.

It was also shown in Ref. [1] that pumping only from one side of the cavity limits the maximum launched pump power due to high thermal load on the heavily doped fiber. Alternatively, the maximum temperature reached at the front end of the active fiber can be significantly reduced by pumping the cavity from both ends, so that they now share the pump heat load. In addition to this, using a longer wavelength pump source also helps to reduce ground state absorption (GSA) and excited state absorption (ESA), which have a significant impact on the temperature increase of the gain fiber [19].

In this Letter, we report a 41.6 W splice-less passively cooled fiber laser cavity operating at 2824 nm. Intracavity splices are avoided by writing both FBGs into the core of the gain fiber, through the polymer coating, using femtosecond pulses at 800 nm and the scanning phase-mask technique. The laser cavity is pumped at 980 nm in both directions simultaneously (bidirectional pumping) to distribute the heat load in the active fiber. This result represents an eightfold increase in average power compared to previous splice-less laser demonstrations operating in this spectral band. The performance of different endcaps is also evaluated and shows that fiber tip degradation is currently the main limitation for further power scaling.

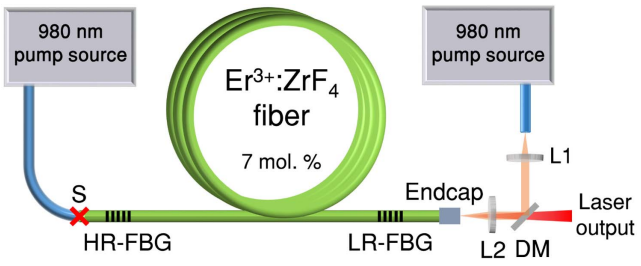

Fig. 1. Experimental setup of the 42 W fluoride fiber laser at 2.824 μm. S, fusion splice between SiO_2 and Er^{3+}:ZrF_4 fibers; HR-FBG, highly reflective grating ($R > 99\%$); LR-FBG, low reflective grating ($R = 8\%$); DM, dichroic mirror; L1 and L2, coupling lenses.

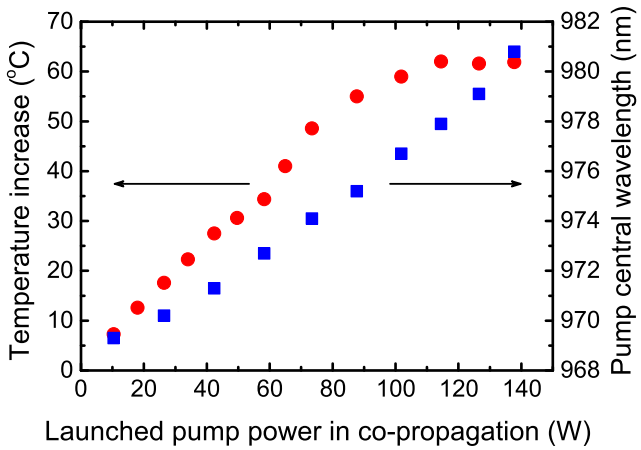

Fig. 2. Maximum temperature increase of the Er^{3+}:ZrF_4 polymer jacket (red dots), along with the pump central wavelength (blue squares) with respect to launched pump power.

The experimental setup of the laser is shown in Fig. 1. A piece of 6.5 m length of 7 mol. % erbium-doped zirconium fluoride ($Er^{3+}:ZrF_4$) double-clad fiber provided by *Le Verre Fluoré* is used as the gain medium of the laser cavity. The fiber core has a 15 μm diameter with a numerical aperture (NA) of 0.12, in agreement with a measured cutoff wavelength of around 2.4 μm. The fiber cladding has a truncated circular geometry with a diameter of 240 × 260 μm and an NA of 0.46. It is pumped from both sides (bidirectional pumping) by two high-power laser diode modules emitting around 980 nm at maximum power. These pump modules are composed of several multi-mode diodes combined in a tapered fused bundle and provide, respectively, ∼145 W and ∼55 W of total continuous output power for the forward and backward side, into 220/240 μm, 0.22 NA multi-mode silica fibers, respectively. On the front end, the silica pump fiber is spliced to the fluoride fiber (*S* in Fig. 1) with a technique described in Ref. [20]. Free-space pumping at the rear end is realized using a pair of ZnSe aspheric lenses (L1 and L2; $f = 12.7$ mm) with a launching efficiency of 63%, including lens losses, DM losses, and mode coupling efficiency. The maximum launched pump powers into the front and rear ends, therefore, are 137.7 and 34.5 W, respectively. A dichroic mirror ($R > 95\%$ at 980 nm, $T > 96\%$ at 2824 nm) is placed between lenses L1 and L2 to launch the backward pump and to eliminate unabsorbed forward pump.

Two FBGs with respective reflectivity of ≥99.5% (HR-FBG) and 8% (LR-FBG) are written in the core of the $Er^{3+}:ZrF_4$ fiber by using a 800 nm femtosecond laser, as described in Ref. [21]. The FBGs are written directly in the active fiber without removing the protective jacket, a process that preserves most of the pristine fiber's mechanical strength [22]. The $Er^{3+}:ZrF_4$ fiber and its FBGs are conductively cooled on an aluminum spool with a continuous V-groove. In addition, the thermal contact with the spool is ensured by applying a thin layer of UV-curable low-index fluoroacrylate polymer on the whole cavity assembly. An AlF_3-based multi-mode fiber segment ($L \approx 650$ μm) with a 400 μm core size from *Fiberlabs* is used as an endcap in order to slow down OH diffusion in the fiber tip [23]. To fabricate the endcap, a long segment of AlF_3 fiber was first spliced to the gain fiber using a filament-based splicer (Vytran GPX-3000). Then the spliced fiber was cleaved with a length of 650 μm and a 4° angle to reduce broadband feedback from the output fiber tip. The losses brought by the splicing are less than 1% in such a procedure. It is then fixed in a copper V-groove filled with low-index fluoroacrylate polymer ($n = 1.36$) to provide pump guiding from the backward side. A copper plate was also placed on top of the fiber tip to provide efficient conduction cooling and to reduce the temperature increase due to backward pumping. During laser operation, the output fiber facet was continuously purged from moisture by blowing an ultra-pure nitrogen flux on the fiber tip to further slow down its degradation due to OH migration.

Direct FBGs writing in the gain fiber of a high-power system imposes some design constraints, particularly when fluoride glass fibers are used. In fact, the low glass transition temperature of fluoride glasses ($Tg \approx 260$°C) leads to a relatively poor thermal stability of the femtosecond written FBGs [21]. For that reason, an appropriate thermal annealing is required to stabilize the FBGs properties at a temperature significantly above the fiber core temperature under strong pumping (i.e., large heat loads). As shown in Fig. 2, the temperature increases of the fiber's jacket surface was monitored with a thermal imaging camera (Jenoptik, Variocam) equipped with a close-up lens. The temperature of the gain fiber's polymer surface reaches a maximum value of about 80°C at the maximum heat load (i.e., at 110 W of launched forward pump power, as seen in Fig. 2) between the fusion splice (*S*) and the HR-FBG. Based on a simple model of heat conduction, the core temperature of the gain fiber is estimated to reach a maximum temperature of about 110°C. Consequently, the FBGs were thermally annealed at 150°C for 10 min to ensure the long-term stability of their performances. Since the annealing process significantly reduces the FBG refractive index modulation, a large initial index modulation (i.e., before annealing) was required to obtain a high reflectivity after annealing. Therefore, designed the HR-FBG of this particularly challenging cavity with a long length ($L = 30$ mm), a uniform period (953 nm), a narrow reflectivity bandwidth (FWHM = 0.9 nm), and a high final reflectivity ($R \geq 99.5\%$). On the other hand, the LR-FBG was written with the same uniform period, but had a much shorter length ($L = 2$ mm) to obtain a low final reflectivity ($R \approx 8\%$), and a relatively large reflectivity bandwidth (FWHM = 1.7 nm) to ensure a good overlap with the HR-FBG during laser operation. Figure 3 shows the transmission spectra of both HR- and

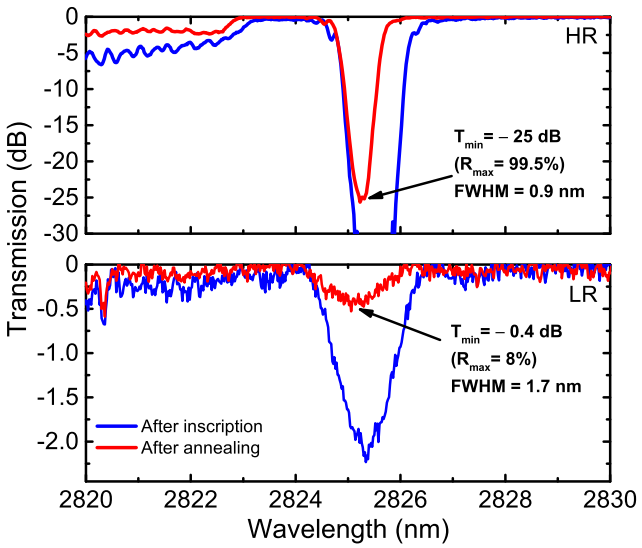

Fig. 3. Transmission spectra of both HR- and LR-FBG after inscription and after thermal annealing at 150°C for 10 min.

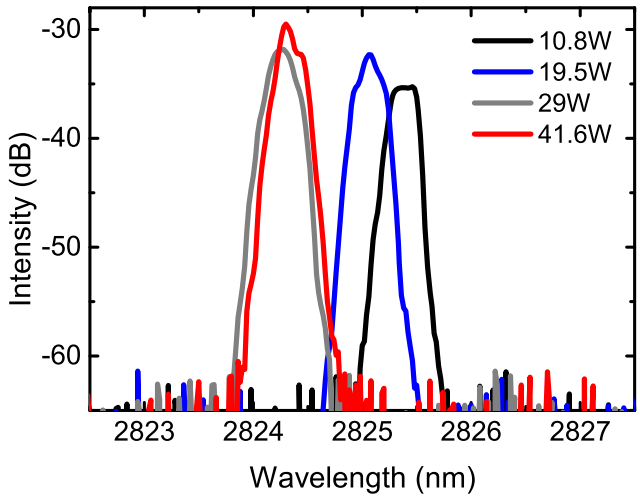

Fig. 5. Output laser spectra measured at 10.8, 19.5, 29, and 41.6 W.

LR-FBGs after inscription and thermal annealing at 150°C for 10 min.

The output power of the laser was measured with a thermopile detector (Gentec UP25N-250F-H12-D0) as a function of the launched pump power (Fig. 4). A maximum of 41.6 W output power is reached when the cavity pumped with 172.2 W of overall (i.e., from both ends) launched pump power around 980 nm. The power of each pump source was increased by the same rate relative to its maximum power to keep the pump wavelength similar from both ends. A slope efficiency of 22.9% is obtained with respect to launched pump power, which is within the typical range for such erbium-doped fiber laser emitting near its maximum gain [13,17].

Output spectra were also recorded for four different powers (10.8, 19.5, 29, and 41.6 W) using a mid-IR optical spectrum analyzer (Yokogawa, AQ6376, spectral resolution set to 0.1 nm) and are shown in Fig. 5. The laser starts to oscillate directly at 2825.3 nm, and its emission wavelength slightly drifts (–25 pm/W) as the output power is increased up to 25 W. This negative spectral drift is due to a thermally induced shift of the HR-FBG center wavelength caused by the negative thermo-optics coefficient of fluoride glasses ($dn/dT \approx -14 \times 10^{-6}$ K^{-1}) [24]. For output powers above 25 W, the lasing wavelength stabilizes near 2823.8 nm. We believe this behavior is explained by the temperature-induced laser diode shift of their central wavelengths from 969 to about 981 nm, as previously shown in Fig. 2. The evolution of the pump central wavelength with respect to the pump power is shown in Fig. 2. As a result, both the GSA and ESA originating from level $^4I_{11/2}$ are significantly reduced. Thus, at sufficiently high pump powers, the local temperature at the front end of the Er^{3+}:ZrF_4 fiber stabilizes so that the HR-FBG central wavelength stops shifting any further. Temperature stabilization of the fiber laser cavity front end was also evidenced in Fig. 2, showing the saturation in the temperature increase of the active fiber's jacket polymer surface. The reduced ESA at high pump levels is also known to have a positive effect on the slope efficiency of the laser, as discussed in Ref. [19]. It is believed that a pump source with a wavelength between 980 and 984 nm would be optimal to keep the temperature of the gain fiber in safe limits and to maximize the slope efficiency of the 2.8 μm transition.

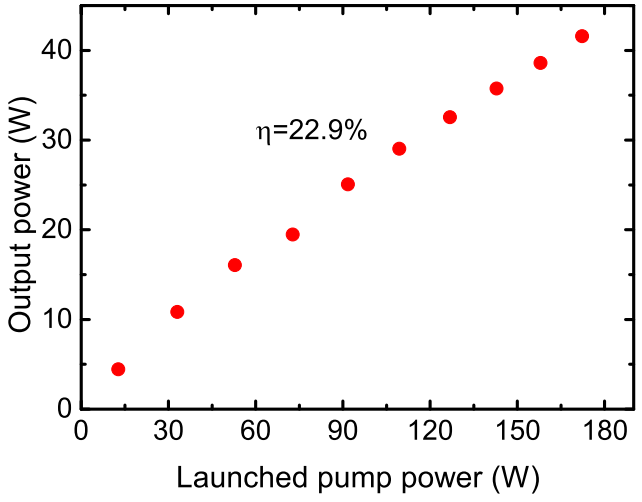

Fig. 4. Measured output power at 2824 nm as a function of the total (forward and backward) launched pump power around 980 nm.

Protective endcaps are key components in 3 μm class lasers to increase the damage threshold associated with OH diffusion in the fiber tip [23] and, thus, ensure long-term operation. Therefore, we proceeded with a long-term laser test while monitoring the temperature of the AlF_3 endcap. For comparison, we also repeated the experiment with an undoped ZrF_4 endcap ($L \approx 650$ μm, $\varnothing core = L \approx 400$ μm) under the same lasing conditions. The tests were performed without nitrogen flux, and the laser cavity was operated at 20 W of average power by pumping from the front end side only. The temperature of the endcaps was recorded with the same thermal camera described above with a 1 s time delay between each temporal data point. The temperature evolution of both AlF_3 and ZrF_4 endcaps as a function of time is shown in Fig. 6(a).

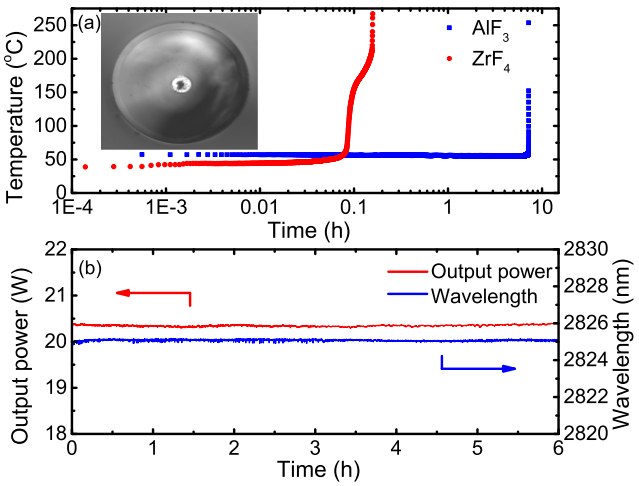

Fig. 6. (a) Temperature evolution of the AlF_3 and ZrF_4 endcaps at 20 W average output power at 2.8 μm, the optical microscope image of AlF_3 tip (inset), and (b) evolution of the output power and central output wavelength near 20 W over a 6 h time period.

Photo-degradation of the AlF_3 endcap was observed after 7 h of continuous operation, whereas this duration was less than 10 min for the ZrF_4 endcap. While AlF_3-based glasses are at least 10 times more resistant to the photodegration process than ZrF_4 glasses [25], these results clearly show that they are still not a good option for long-term operation of high-power fiber lasers near 3 μm. The optical microscope image of the degraded AlF_3 tip is shown in inset of Fig. 6(a), where catastrophic damage due to OH diffusion is clearly observed. In order to achieve higher output powers and long-term stability, other endcap materials that are less permeable to OH contamination need to be considered. For the power scaling, the temperature on the gain fiber could also be reduced by improving the fiber design, either by lowering the Er^{3+} concentration or by reducing the core-clad ratio. Moreover, using a pump source having a fixed operating central wavelength between 980 and 984 nm would help to reduce the thermal load by lowering the GSA and ESA. In the near future, pump combiners might provide an interesting solution for pumping erbium-doped fluoride fiber cavities from both ends with higher pump launching efficiencies while maintaining a heat load to a reasonable level [26]. The output power and central output wavelength near 20 W were also measured during a 6 h stability test. In these measurements, root-mean square fluctuations of 0.09% and 0.014%, respectively, were obtained for the output power and output wavelength [Fig. 6(b)].

In conclusion, we have demonstrated an erbium-doped fluoride glass fiber laser delivering a maximum output power of 41.6 W at 2824 nm using a simple splice-less cavity design. This result is the highest average output power ever achieved from a mid-infrared laser cavity. We showed that fiber tip degradation is still one of the main problems for power scaling and long-term reliability of 3 μm fiber lasers. We also investigated the effect of pump wavelength on the temperature load of the gain fiber. This Letter represents a significant advance for further power scaling of erbium-doped fiber lasers emitting near 3 μm.

Funding. Natural Sciences and Engineering Research Council of Canada (NSERC) (CG101779, CG112389, CG119242); Canada Foundation for Innovation (CFI) (GF072345); Fonds de Recherche du Québec—Nature et Technologies (FRQNT) (CO201310, FT097991).

Acknowledgment. The authors would like to thank Marc D'Auteuil and Stéphan Gagnon for their technical assistance.

REFERENCES

1. V. Fortin, M. Bernier, S. T. Bah, and R. Vallée, Opt. Lett. **40**, 2882 (2015).
2. S. Tokita, M. Murakami, S. Shimizu, M. Hashida, and S. Sakabe, Opt. Lett. **36**, 2812 (2011).
3. S. Duval, M. Bernier, V. Fortin, J. Genest, M. Piché, and R. Vallée, Optica **2**, 623 (2015).
4. M. Murakami, S. Hattori, C. Schaefer, and K. Yahata, in *Proceedings of the 83rd Laser Materials Processing Conference* (2015), p. 117.
5. M. R. Dickinson, A. Charlton, T. A. King, A. J. Freemont, and R. Bramley, Laser Med. Sci. **6**, 125 (1991).
6. H. H. P. T. Bekman, J. C. van den Heuvel, F. J. M. van Putten, and R. Schleijpen, Proc. SPIE **5615**, 27 (2004).
7. S. Jackson, Electron. Lett. **40**, 1400 (2004).
8. M. R. Majewski and S. D. Jackson, Opt. Lett. **41**, 2173 (2016).
9. M. Pollnau, C. Ghisler, G. Bunea, M. Bunea, W. Luthy, and H. P. Weber, Appl. Phys. Lett. **66**, 3564 (1995).
10. S. Tokita, M. Murakami, S. Shimizu, M. Hashida, and S. Sakabe, Opt. Lett. **34**, 3062 (2009).
11. S. D. Jackson, T. A. King, and M. Pollnau, Opt. Lett. **24**, 1133 (1999).
12. Y. O. Aydin, V. Fortin, F. Maes, F. Jobin, S. D. Jackson, R. Vallée, and M. Bernier, Optica **4**, 235 (2017).
13. D. Faucher, M. Bernier, G. Androz, N. Caron, and R. Vallée, Opt. Lett. **36**, 1104 (2011).
14. X. Zhu and R. Jain, Opt. Lett. **32**, 26 (2007).
15. S. Tokita, M. Hirokane, M. Murakami, S. Shimizu, M. Hashida, and S. Sakabe, Opt. Lett. **35**, 3943 (2010).
16. V. Fortin, M. Bernier, N. Caron, D. Faucher, M. El-Amraoui, Y. Messaddeq, and R. Vallée, Proc. SPIE **8601**, 86011H (2013).
17. M. Bernier, D. Faucher, N. Caron, and R. Vallée, Opt. Express **17**, 16941 (2009).
18. D. Faucher, M. Bernier, N. Caron, and R. Vallée, Opt. Lett. **34**, 3313 (2009).
19. J. Li and S. D. Jackson, IEEE J. Quantum Electron. **48**, 454 (2012).
20. H. Okamoto, K. Kasuga, and Y. Kubota, Opt. Lett. **36**, 1470 (2011).
21. M. Bernier, D. Faucher, R. Vallée, A. Saliminia, G. Androz, Y. Sheng, and S. L. Chin, Opt. Lett. **32**, 454 (2007).
22. M. Bernier, F. Trépanier, J. Carrier, and R. Vallée, Opt. Lett. **39**, 3646 (2014).
23. N. Caron, M. Bernier, D. Faucher, and R. Vallée, Opt. Express **20**, 22188 (2012).
24. J. M. Jewell and I. D. Aggarwal, J. Non-Cryst. Solids **142**, 260 (1992).
25. G. Frischat, B. Hueber, and B. Ramdohr, J. Non-Cryst. Solids **284**, 105 (2001).
26. C. A. Schäfer, H. Uehara, D. Konishi, S. Hattori, H. Matsukuma, M. Murakami, S. Shimizu, and S. Tokita, Opt. Lett. **43**, 2340 (2018).